Resonant Frequency and Quality Factors of a Silver-Coated $\lambda/4$ Dielectric Waveguide Resonator

Arun Chandra Kundu, *Student Member, IEEE,* and Ikuo Awai, *Member, IEEE*

***Abstract*— In this paper, resonant frequency, radiation loss, conductor loss, and dielectric loss of a silver-coated $\lambda/4$ dielectric waveguide resonator are investigated. Leakage of the electromagnetic field from the open-end face of the resonator is the only source of radiation, which also affects the resonant frequency. New theoretical expressions are devised to calculate resonant frequency, conductor quality (Q) factor, dielectric Q factor, and radiation Q factor. Effective conductivity of the resonator-coated silver is estimated from experimental unloaded Q factor. The theoretical analysis is validated by the experimental result and the data obtained using the finite-difference time-domain (FDTD) technique. Finally, we have designed and fabricated a dual-mode bandpass filter using this resonator.**

***Index Terms*—Dielectric waveguide resonator, high permittivity, radiation Q factor, resonant frequency, unloaded Q factor.**

I. Introduction

CELLULAR mobile-communication systems are expanding rapidly throughout the world, and a number of terminals and small base stations for these systems have been rapidly increasing. One of the most important components widely used are dielectric resonator filters. These resonators demand high dielectric constant to enable compact design, low dielectric loss to offer high quality (Q) factor, and good stability on the temperature. Silver is considered as the coating metal since it hold the highest conductivity among metals.

Since Q factors are important parameters which indicate the property of a resonator, a thorough investigation is made on resonant frequency and Q factors of a $\lambda/4$ dielectric waveguide resonator that has an open-end face (OEF). This resonator is of square cross section, which allows dual degenerate modes. We can make the optimum use of the OEF of a $\lambda/4$ resonator for coupling of the dual modes, coupling to the external circuit, and tuning the frequency of each mode [1].

In principle, the OEF of the resonator radiates energy and, thus, unloaded Q substantially degrades. Thus, the estimation of radiation loss and study on the condition to reduce it are the most important factors for versatile use of a $\lambda/4$ dielectric waveguide resonator. Due to leakage of the electromagnetic field from the OEF, the perfect magnetic wall (PMW) is shifted from the OEF into the interior of the resonator, and effective wavelength of the resonator decreases. As a result, resonant frequency increases. We will derive new equations to explain the experimental resonant frequencies of $\mathrm{TE}_{\mathrm{mnp}}$- and $\mathrm{TM}_{\mathrm{mnp}}$-like modes. We will also derive new equations to calculate the conductor Q factor, dielectric Q factor, and radiation Q factor by using waveguide approximation and comparing it with finite-difference time-domain (FDTD) analysis data.

We will separately analyze the electric- and magnetic-field distribution of a $\lambda/4$ resonator by FDTD simulation. We will also compare all the theoretical and experimental results with the FDTD simulation data. In the final section, we will design and fabricate a dual-mode bandpass filter using a single $\lambda/4$ resonator having a dimension of 5 mm $\times$ 5 mm $\times$ 10 mm.

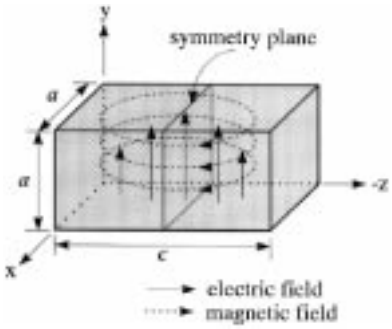

Fig. 1. Electromagnetic-field distribution for TE_{101} mode of a $\lambda/2$ resonator.

II. Dual Mode in a $\lambda/4$ Dielectric Waveguide Resonator

A directly silver-coated $\lambda/2$ dielectric waveguide resonator of square cross section has two lowest degenerate orthogonal modes TE_{101} and TE_{011}, which are perpendicular to each other. They couple through a perturbation which destroys the symmetry and splits resonant frequencies. Now, if we cut a $\lambda/2$ resonator along its symmetry plane (see Fig. 1), about which the electric field of the dominant mode is symmetric, we can get two quarter-wavelength resonators.

Due to high relative permittivity of 93, the field confinement is strong enough, and the field distribution of a $\lambda/4$ dielectric waveguide resonator should not significantly differ from that of a $\lambda/2$ resonator. Hence, we named these fundamental modes the TE'_{101} and TE'_{011} modes after the TE_{101} and TE_{011} modes of a $\lambda/2$ resonator. The electric-field distribution of a $\lambda/4$ resonator is shown in Fig. 2. The degenerate modes

Manuscript received September 1, 1997; revised February 5, 1998.

The authors are with the Department of Electrical Engineering, Yamaguchi University, 2557 Tokiwadai, Ube-755, Japan.

Publisher Item Identifier S 0018-9480(98)05507-0.

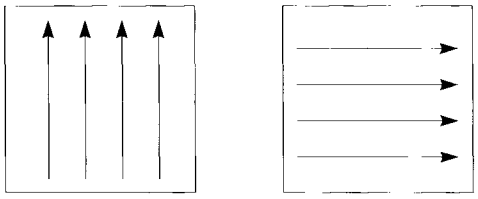

Fig. 2. Electric-field distribution of two degenerate modes at the OEF of the resonator.

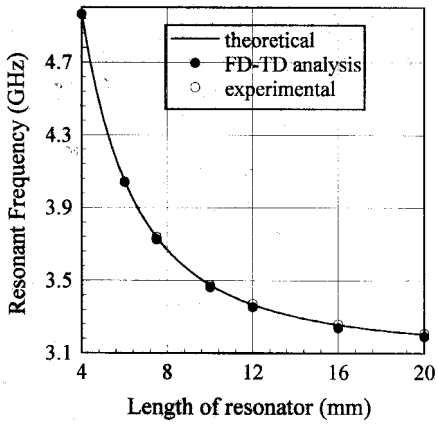

Fig. 3. Comparison of theoretical, measured, and analytical resonant frequencies of $\lambda/2$ resonators (resonator dimension: 5 mm $\times$ 5 mm $\times$ 20 mm, $\epsilon_r = 93$).

are utilized for fabricating a miniaturized bandpass filter with space-effective configuration. The cross section of the resonator will be taken as 5 mm $\times$ 5 mm.

III. Resonant Frequency

For $\lambda/2$ resonators, the experimental resonant frequencies show an excellent agreement with theoretical and FDTD analytical values, as shown in Fig. 3. From Fig. 3, we can also justify the validity of our FDTD program. For $\lambda/4$ resonators, the experimental and theoretical resonant frequencies differ to a significant amount. It is because the resonant frequency of a $\lambda/4$ dielectric waveguide resonator was calculated by considering its open-end face (OEF) as a PMW. In reality, it is not true, since a portion of the electromagnetic field leaks from the OEF, and effective wavelength (λ_g) in the resonator becomes shorter than the physical length, as shown in Fig. 4, and naturally, the experimental resonant frequency becomes higher than that of the theoretical ones. Focusing attention on this point, a new concept is proposed to calculate the resonant frequency of a $\lambda/4$ dielectric waveguide resonator by using waveguide approximation as follows.

Let us suppose that there exists an infinitely long air-filled waveguide in contact with the OEF of a $\lambda/4$ dielectric waveguide resonator, as shown in Fig. 5. If Z_0 is the characteristics impedance of the air-filled waveguide and $Z_{\rm in}$ is the input impedance looking into the dielectric-filled waveguide, the condition for resonance of the dielectric waveguide resonator

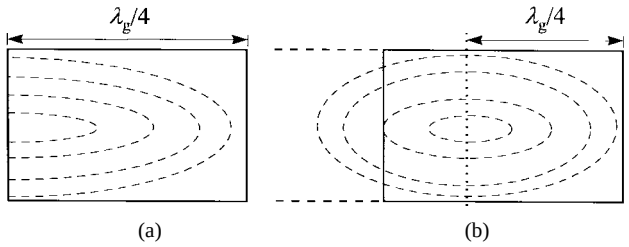

Fig. 4. Electromagnetic-field distribution at the OEF of a $\lambda/4$ resonator. (a) PMW approximation. (b) Waveguide approximation.

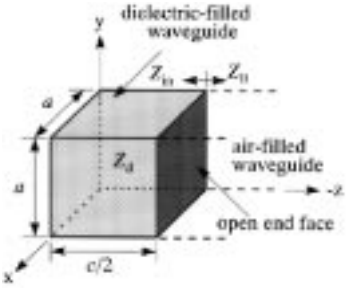

Fig. 5. Infinitely long air-filled waveguide in contact with the OEF of the dielectric-filled waveguide.

becomes

$$Z_{\rm in} + Z_0 = 0 \tag{1}$$

where $Z_{\rm in} = jZ_d \tan(\beta c/2)$ and c is the length of a $\lambda/2$ dielectric waveguide resonator.

From (1), we can deduce the following relations to calculate the resonant frequencies of $\mathrm{TE}'_{\rm mnp}$ and $\mathrm{TM}'_{\rm mnp}$ modes, respectively,

$$\left[\left\{\omega_0^2\varepsilon_0\varepsilon_r\mu_0 - \left(\frac{m\pi}{a}\right)^2 - \left(\frac{n\pi}{a}\right)^2\right\}^{1/2} c/2\right] - \tan^{-1}\left[-\left\{\frac{\omega_0^2\varepsilon_0\varepsilon_r\mu_0 - \left(\frac{m\pi}{a}\right)^2 - \left(\frac{n\pi}{a}\right)^2}{\left(\frac{m\pi}{a}\right)^2 + \left(\frac{n\pi}{a}\right)^2 - \omega_0^2\varepsilon_0\mu_0}\right\}^{1/2}\right] = 0 \tag{2}$$

and

$$\left[\left\{\omega_0^2\varepsilon_0\varepsilon_r\mu_0 - \left(\frac{m\pi}{a}\right)^2 - \left(\frac{n\pi}{a}\right)^2\right\}^{1/2} c/2\right] - \tan^{-1}\left[\varepsilon_r\left\{\frac{\left(\frac{m\pi}{a}\right)^2 + \left(\frac{n\pi}{a}\right)^2 - \omega_0^2\varepsilon_0\mu_0}{\omega_0^2\varepsilon_0\varepsilon_r\mu_0 - \left(\frac{m\pi}{a}\right)^2 - \left(\frac{n\pi}{a}\right)^2}\right\}^{1/2}\right] = 0 \tag{3}$$

where a is a side length of the square cross section of the resonator. Now, the resonant frequency of the TE'_{101} mode for various lengths of the resonator, calculated by (2), is shown in Fig. 6. From Fig. 6, we see that the results obtained by theoretical analysis, the FDTD method, and a laboratory test are in good agreement with each other.

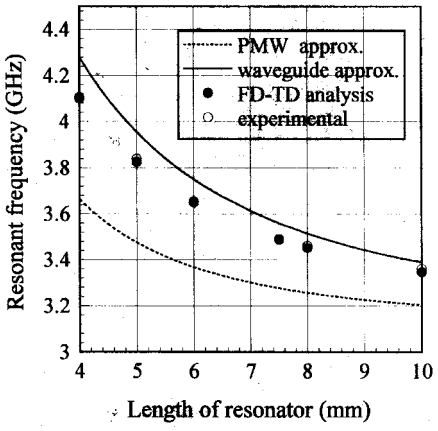

Fig. 6. Resonant frequency versus length of $\lambda/4$ resonator (resonator dimension: 5 mm $\times$ 5 mm $\times$ 10 mm, $\varepsilon_r = 93$).

TABLE I

Mode	Calculated (GHz)	Measured (GHz)	FD-TD analysis (GHz)
TE'_{011} 101	3.389	3.360	3.346
TE'_{012} 102	4.149	4.069	4.069
TE'_{111}	4.614	4.586	4.568
TE'_{103} 013	5.223	5.131	5.134
TE'_{112}	5.225	5.142	5.137
TE'_{021} 201	6.082	6.034	6.037
TE'_{104} 014	6.478	6.397	6.382
TE'_{121}	7.101	7.003	7.001
TE'_{105} 015	7.833	7.768	7.737

Here, we also observe that the theoretical resonant frequencies calculated by first-order approximation exists at a little bit higher than the experimental values. It is because we have considered an infinitely long air-filled waveguide in contact with the OEF of the resonator. In reality, it is not a waveguide, but free space. Thus, the evanescent field should be spreading more to reduce the frequency shift from the first-order result.

The resonant frequencies of higher order TE'_{mnp} and TM'_{mnp} modes, including dominant modes of a 5 mm $\times$ 5 mm $\times$ 10 mm $\lambda/4$ dielectric waveguide resonator calculated by the first-order approximation, are shown in Tables I and II. From these tables, we have identified all the experimentally obtained resonant modes (see Fig. 7) of a $\lambda/4$ resonator of the same dimension, and verified them with the FDTD analytical values. They have shown a very good agreement.

IV. Field Analysis by FDTD Method

A. Simulation Technique of Resonant Frequency and Q Factors of a $\lambda/4$ Resonator by the FDTD Method

By fast Fourier transformation (FFT) of the time-step response of the resonator, we can obtain the resonant frequency spectrum. For the high Q-resonator, we can accurately compute the Q factors by the FDTD perturbation method [2]. Using the theoretical equations and discretizing its integration, the Q factors can be expressed as follows:

TABLE II

Mode	Calculated (GHz)	Measured (GHz)	FD-TD analysis (GHz)
TM'_{111}	4.46445	4.468	4.456
TM'_{112}	4.975	4.98	4.963
TM'_{113}	5.864	5.875	5.849
TM'_{121} 211	6.994	7.018	6.932
TM'_{122} 212	7.363	7.323	7.24

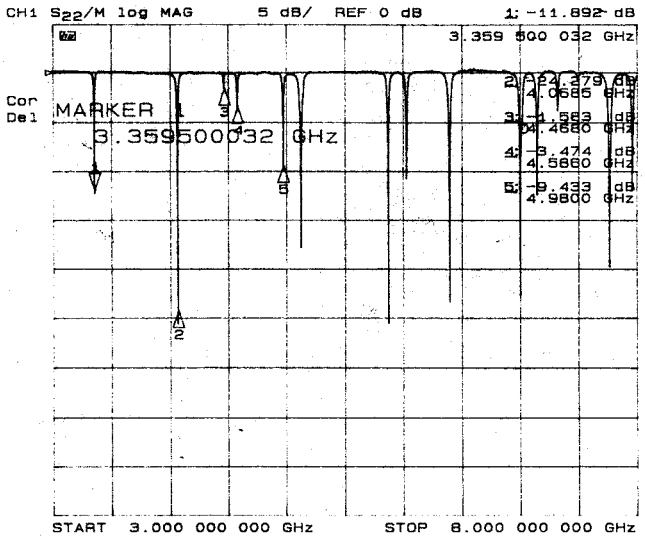

Fig. 7. Higher order modes including the dominant mode of a 5 mm $\times$ 5 mm $\times$ 10 mm $\lambda/4$ resonator.

$$Q_c = \omega_0 \frac{W}{P_c} = \frac{2}{\delta} \frac{\int_V |H|^2 \, dV}{\oint_S |H_t|^2 \, dS} \tag{4}$$

$$Q_d = \omega_0 \frac{W}{P_d} = \frac{\int_V \varepsilon |E|^2 \, dV}{\int_{V'} \varepsilon'' |E|^2 \, dV'} \tag{5}$$

where Q_c and Q_d are the conductor and dielectric Q factor of the resonator, ε'' is the imaginary part of the dielectric medium, W is the average stored energy, P_c and P_d are, respectively, the average dissipated power by conductor wall and dielectric of the resonator, and V denotes the volume of the resonator plus volume of the metal box, which is placed in contact with the OEF of a $\lambda/4$ dielectric waveguide resonator. V' denotes the volume of the dielectric resonator only, ω_0 is the angular resonant frequency, H_t is the magnetic field tangential to the conductor wall, and δ is the depth of penetration of the conductor wall.

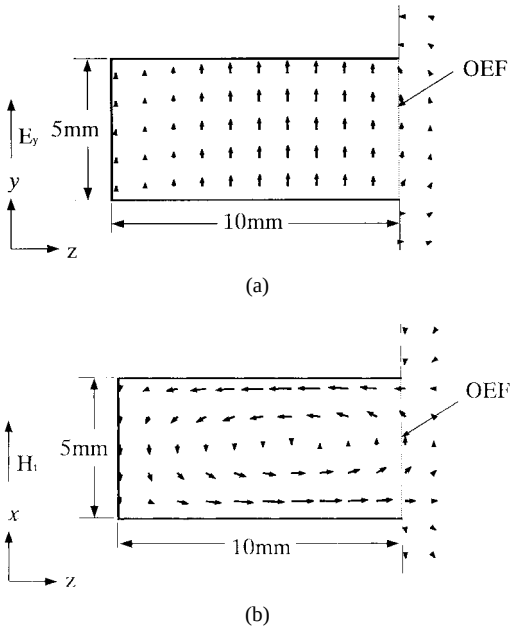

Fig. 8. (a) E_y component of the electric field of TE'_{101} mode in y–z plane of the resonator. (b) Transverse magnetic field of the resonator in x–z plane of the resonator.

In the FDTD analysis, the resonator is excited by the following Gaussian modulated radio-frequency (RF) pulse and the center frequency is set to the resonant frequency [3]

$$H_x = \exp[-(\Delta t \cdot n - 3T)^2/T^2] \tag{6}$$

where $\Delta t = 0.68$ ps, $T = 1.8734$ ns, and n is the step number.

In our analysis, we have added a 20 mm × 20 mm × 30 mm metal box on the top space of the resonator, which will suppress the radiation loss.

The radiation Q factor Q_r can be simulated by using the following equation, which have been devised from the basic equation of the Q factor [4]:

$$Q_r = \frac{\omega_0}{\ln\ a} t \tag{7}$$

where α is the ratio of attenuated stored energy for period t.

To compute the radiation Q factor, the super-absorbing second-order Mur absorbing boundary conditions (ABC's) are utilized instead of the metal box, used for calculation of Q_c and Q_d. This condition simulates the open space extending to infinity, and can suppress the spurious reflections of outward-propagating numerical-wave modes at the OEF truncations by 99.9% [5]. The time-step function will be attenuated at the observation point, which is taken very close to the OEF. From the time-step function, we can determine α by calculating the ratio of average electric or magnetic energy for a certain period of t.

B. Analysis of Electromagnetic Field of a $\lambda/4$ Resonator by the FDTD Method

The E_y component of the electric field inside and at the OEF of the resonator, simulated by the FDTD technique, is shown in the y–z plane of Fig. 8(a). Similarly, the tangential component of the magnetic field (H_t) is shown in the x–z plane of Fig. 8(b). For more clarification, the amplitude of the E_y component is also shown in a three-dimensional (3-D) form in Fig. 9. From these figures, it is clear that a small portion of the electromagnetic field leaks from the OEF and the shift of the PMW is (maximum E_y plane) quite large considering a little leakage of the field.

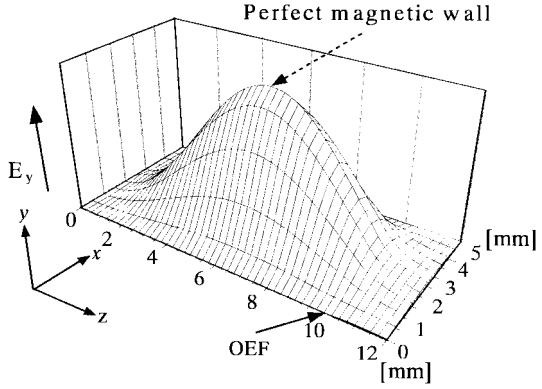

Fig. 9. E_y field component inside a 5 mm × 5 mm × 10 mm $\lambda/4$ resonator.

V. Theory on Conductor, Dielectric, and Unloaded Q Factors of Resonator

A. Q_c and Q_d Values of $\lambda/2$ Resonator

The conductor Q factor Q_c and the dielectric Q factor Q_d for the TE_{101} mode of a $\lambda/2$ rectangular dielectric waveguide resonator can be obtained from the following equations:

$$\begin{aligned} Q_C &= \frac{1}{\delta\lambda_0^2}\,\frac{4a^3c^3}{c(a^2+c^2)+2(a^3+c^3)} \\ &= \frac{1}{\delta}\,\frac{a(a^2+c^2)}{(a^2+c^2)+\dfrac{2}{c}(a^3+c^3)} \end{aligned} \tag{8}$$

$$Q_d = \frac{A}{f_o} = \frac{1}{\tan\delta} \tag{9}$$

where λ_0 is the free-space wavelength of a half-wavelength resonator δ (skin depth of the silver coating) $= (1/\sqrt{\pi f_0 \mu_0 \sigma_1})$, $\sigma_1 = s\sigma_0$, σ_0 is the conductivity of the bulk silver, s is the multiplication factor, and A is the loss factor of the dielectric material and is independent of frequency [6]. Its measured value is given by Ube Industries, Ube, Japan, to be 6000 GHz, f_0 is the resonant frequency, and c, a are the length and width of the resonator, respectively. The simulated and theoretical Q_c and Q_d values are depicted in Fig. 10, which shows an excellent agreement. During the calculation and simulation of Q_c, $s = 0.6$ was taken into account.

B. Determination of Effective Conductivity of the Silver Coating

The unloaded Q factor Q_0 of a $\lambda/2$ rectangular dielectric waveguide resonator can be calculated by using the following equation:

$$\frac{1}{Q_0} = \frac{1}{Q_c} + \frac{1}{Q_d}. \tag{10}$$

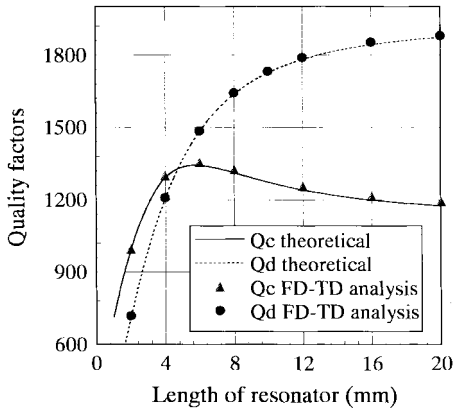

Fig. 10. Theoretical and analytical Q_c and Q_d values for half-wavelength resonator.

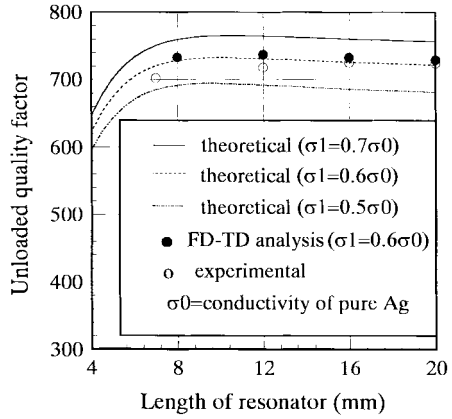

Fig. 11. A comparative study of theoretical, analytical, and measured Q_0 values for a $\lambda/2$ resonator.

The measured, calculated, and analytical Q_0 versus length of a $\lambda/2$ resonator is shown in Fig. 11. From the comparison of theoretical and measured Q_0 values, we have tried to find out the effective conductivity of the resonator-coating silver. Due to surface roughness of the resonator and frit in the silver paste, the electric-current flow is hampered. As a result, Q_0 values decrease. From Fig. 11, we see that both values are in coincidence for $\sigma_1 = 0.6\sigma_0$ [7]. This value was used for the theoretical calculation of Q_c of a $\lambda/4$ resonators.

C. Q_c and Q_d Values of $\lambda/4$ Resonator

With the help of the waveguide concept, we have defined the field components of TE'_{101} mode inside a $\lambda/4$ resonator as follows:

$$E_y = E_0 \sin\left(\frac{\pi x}{a}\right)\sin(\beta z) \tag{11}$$

$$H_x = \frac{E_0\beta}{j\omega_0\mu_0}\sin\left(\frac{\pi x}{a}\right)\cos(\beta z) \tag{12}$$

$$H_z = \frac{jE_0}{\omega_0\mu_0}\left(\frac{\pi}{a}\right)\cos\left(\frac{\pi x}{a}\right)\sin(\beta z) \tag{13}$$

where E_0 is a constant and $\beta^2 = \omega_0^2\varepsilon_0\varepsilon_r\mu_0 - (\pi/a)^2$.

By applying the boundary conditions at the OEF, we can deduce the electromagnetic-field components of the air-filled waveguide, shown in Fig. 5, which are given below:

$$E'_y = E_0 \sin\left(\frac{\beta c}{2}\right)\sin\left(\frac{\pi x}{a}\right)e^{-\gamma(z-c/2)} \tag{14}$$

$$H'_x = \frac{-E_0\gamma}{j\omega_0\mu_0}\sin\left(\frac{\beta c}{2}\right)\sin\left(\frac{\pi x}{a}\right)e^{-\gamma(z-c/2)} \tag{15}$$

$$H'_z = \frac{jE_0}{\omega_0\mu_0}\left(\frac{\pi}{a}\right)\sin\left(\frac{\beta c}{2}\right)\cos\left(\frac{\pi x}{a}\right)e^{-\gamma(z-c/2)} \tag{16}$$

where $\gamma^2 = (\pi/a)^2 - \omega_0^2\varepsilon_0\mu_0$.

We have elucidated the conductor Q factor as follows:

$$Q_c = \omega_0\frac{(W_1+W_2)}{P_c} = \frac{8a\pi^2}{\delta\lambda_{01}^2} \times \left[\frac{\dfrac{\varepsilon_r}{2}\left(c-\dfrac{1}{\beta}\sin\beta c\right)+\dfrac{\sin^2\left(\dfrac{\beta c}{2}\right)}{\gamma}}{3c\left(\dfrac{\pi}{a}\right)^2+\sin\beta c\left\{\beta-\dfrac{3}{\beta}\left(\dfrac{\pi}{a}\right)^2+\beta^2(c+2a)\right\}}\right] \tag{17}$$

where λ_{01} is the free-space wavelength of a $\lambda/4$ resonator, W_1 denotes the total energy stored within the dielectric-filled waveguide, and W_2 is the total energy stored within the air-filled waveguide.

We have also devised the following equation for the dielectric Q factor:

$$Q_d = \frac{(W_1+W_2)}{P_d} = \frac{\displaystyle\int_{V''}\varepsilon_0|E|^2\,dV'' + \int_{V'}\varepsilon|E|^2\,dV'}{\displaystyle\int_{V'}\varepsilon''|E|^2\,dV'} = \frac{1}{\tan\delta}\left[1+\frac{1}{\varepsilon_r}\frac{2\sin^2\left(\dfrac{\beta c}{2}\right)}{\gamma\left(c-\dfrac{1}{\beta}\sin(\beta c)\right)}\right] \tag{18}$$

where V'' is the volume of the air-filled waveguide, $\varepsilon(\omega_0) = \varepsilon' - j\varepsilon''$, in which ε' contributes to the stored energy, $\omega_0\varepsilon''$ contributes to the power dissipation, and $\tan\delta = \varepsilon''/\varepsilon'$ [8].

The Q_c and Q_d values calculated by using (17) and (18) and those calculated by PMW approximation are compared with FDTD simulated data, and are depicted in Fig. 12, which shows that the Q_c and Q_d values calculated by waveguide approximation exhibits a close proximity with the FDTD data, especially when the length of the resonator becomes larger. It seems physically reasonable since the leakage of the fields decreases according to the length of the resonator.

VI. Radiation Q Factor

We have measured the radiation Q factor Q_r based on the expectation that Q_c and Q_d are almost the same for both $\lambda/2$ and $\lambda/4$ resonators. Since all the surfaces of a $\lambda/2$ resonator are directly silver coated, there is no radiation loss. Thus, if we

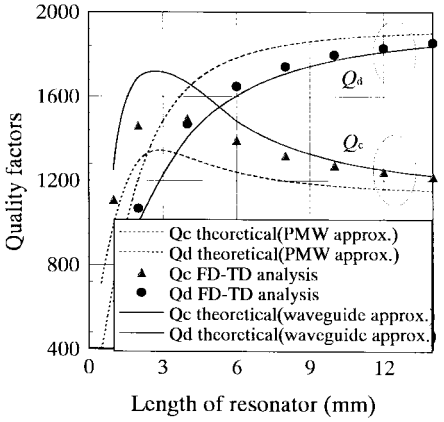

Fig. 12. Q_c and Q_d versus length of the resonator for $\lambda/4$ resonator.

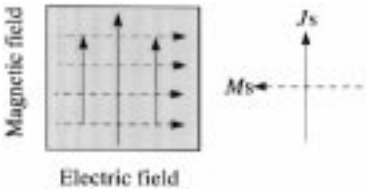

Fig. 13. Explanation of electromagnetic surface current.

subtract the $1/Q_0$ values of $\lambda/2$ from that of a $\lambda/4$ resonator, we can measure the Q_r values. The assumption above is not valid examining the difference of the FDTD result for $\lambda/2$ and $\lambda/4$ resonators, shown in Figs. 10 and 12, respectively. Fortunately, however, the sum $(1/Q_c)+(1/Q_d)$ is almost the same for each resonator and, hence, the extraction of Q_r from the measured data for each Q_0 becomes possible.

According to Konishi [9], we can replace the electric field of the OEF of a $\lambda/4$ resonator by a magnetic surface current M_s. The derived P_r and Q_r by M_s are given as

$$P_r = \frac{8}{3\pi}\,\frac{a^4}{\lambda_0^2}\,\frac{E_0^2}{\eta_0} \tag{19}$$

$$Q_r = \frac{3\pi^2}{32}\,\frac{c\lambda_0}{a^2}\varepsilon_r \tag{20}$$

where P_r is the radiated power, Q_r is the radiation Q factor, λ_0 is the free-space wavelength, and η_0 is the free-space intrinsic impedance.

However, Q_r values calculated from (20) are too large to explain the measured values (for $c/2 = 10$ mm, $Q_r \cong 6000$), since (20) was derived by considering the OEF of a $\lambda/4$ resonator as a PMW. In reality, a PMW is possible only when $\varepsilon_r = \infty$. However, until today, that of commercially available dielectric ceramics is less than 100. As a result, magnetic-field leaks from the OEF and PMW are shifted into the interior of the resonator, as shown in Fig. 4.

Thus, the tangential component of the magnetic field exists at the OEF, in addition to the tangential electric field. This magnetic field causes an effective electric-current source (J_s) at the OEF and assists in increasing the radiation loss, as shown in Fig. 13.

By analyzing these electromagnetic fields on the OEF, we have derived the following equation to calculate the radiation

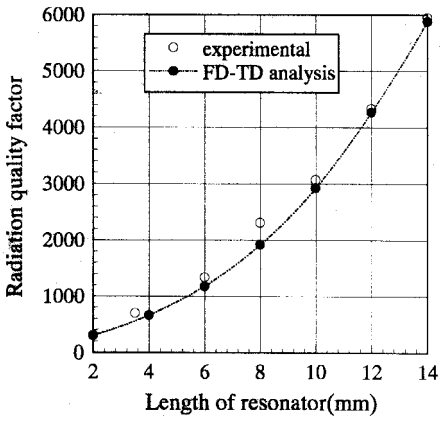

Fig. 14. Comparison of experimental and analytical radiation Q factors of a $\lambda/4$ resonator.

Q factor:

$$Q_r = \frac{\omega_0(W_1+W_2)}{P_r} = \frac{3\pi^4}{8\lambda_{01}a^2}\,\frac{\left[\varepsilon_r\left\{c-\frac{1}{\beta}\sin(\beta c)\right\}+\frac{2}{\gamma}\sin^2(\beta c)\right]}{\left[\beta^2\cos^2\left(\frac{\beta c}{2}\right)+\frac{4\pi^2}{\lambda_{01}^2}\sin^2\left(\frac{\beta c}{2}\right)\right]} \tag{21}$$

where W_1 denotes the total energy stored within the dielectric-filled waveguide and W_2 is the total energy stored within the air-filled waveguide.

However, the Q_r values obtained from (21) were too small (for $c/2 = 10$ mm, $Q_r \cong 1000$) to explain the measured values. Thus, we have simulated the radiation Q factor by the FDTD technique, which shows a good agreement with the measured values, as shown in Fig. 14.

VII. Unloaded Q Factor of a $\lambda/4$ Resonator

Unloaded Q factor Q_0 of a $\lambda/4$ resonator may be written as follows:

$$\frac{1}{Q_0} = \frac{1}{Q_c} + \frac{1}{Q_d} + \frac{1}{Q_r}. \tag{22}$$

The experimental Q_0 values and the FDTD results shown in Figs. 12 and 14 summed by use of (22) are shown in Fig. 15. From Fig. 15, we see that the experimental Q_0 values of $\lambda/4$ resonators are in good agreement with the numerical ones. It is also observed that, for the resonator length larger than around 10 mm, the Q_0 values have little increment. In addition, the resonant frequency does not effectively decrease above 10 mm, as shown in Fig. 6. Thus, around 10 mm would be the most effective length, considering tradeoff of Q_0 and volume for the resonator of 5 mm $\times$ 5 mm cross section [1]. Therefore, it would be recommended to change the cross-sectional dimension a so as to have a resonator of different resonant frequency.

Recalling (2), the resonant wavelength becomes proportional to a if one also increases c proportional to a, and it seems a rule of thumb to keep the ratio of the length to the

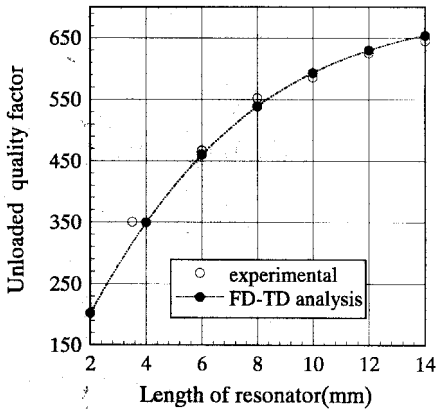

Fig. 15. Comparison of experimental and analytical unloaded Q factors of a $\lambda/4$ resonator.

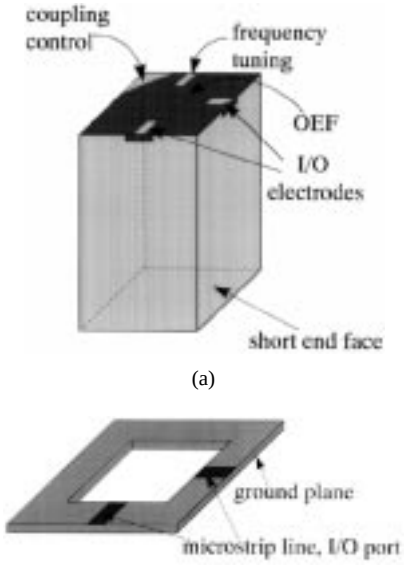

Fig. 16. (a) Configuration of a dual-mode bandpass filter. (b) Printed circuit board for strip-line excitation.

width equal to two. However, the various Q values calculated by (17)–(21) give the following dependence on a under the condition $c \propto a$:

$$Q_c \propto \sqrt{a}, \quad Q_d \propto a \quad Q_r = \text{constant}. \tag{23}$$

Hence, the tradeoff point mentioned above will shift slightly according to the resonant frequency, though the rule of thumb holds for a wide microwave frequency band.

VIII. Design and Fabrication of Dual-Mode BPF

A dual-mode BPF is designed with the help of the insertion-loss method. The normalized reactances of a maximally flat two-stage prototype low-pass filter is given as [10]

$$g_0 = g_3 = 1 \quad g_1 = g_2 = 1.414. \tag{24}$$

If we choose the center frequency $f_0 = 3.36$ GHz and bandwidth $B = 120$ MHz, the coupling constant is

$$k = \frac{1}{\sqrt{g_1 g_2}} \frac{B}{f_0} = 0.025. \tag{25}$$

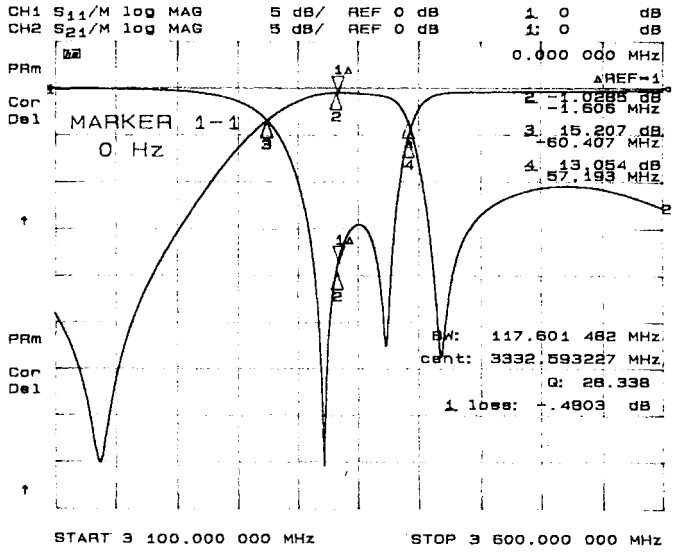

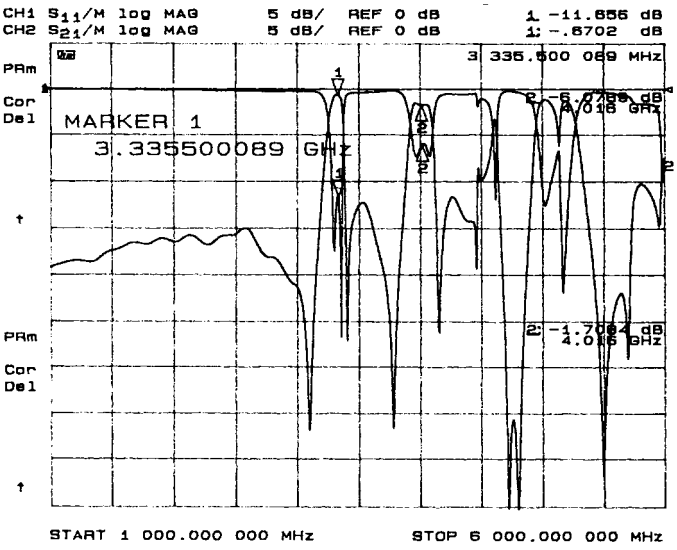

Fig. 17. Measured frequency response of the dual-mode bandpass filter. (a) Transmission and return loss. (b) Spurious response.

As for the external Q factor (Q_e),

$$Q_e = \frac{g_0 g_1 f_0}{B} = 39.6. \tag{26}$$

The filter configuration is shown in Fig. 16(a). It is mounted through the 5 mm $\times$ 5 mm hole of the printed circuit board [see Fig. 16(b)]. Here, the input/output loads are achieved via microstrip lines. The coupling between the degenerate modes is controlled by the size of the triangular metal pattern at the OEF, and external Q factor is controlled by the dimension of the exciting electrode [1].

The insertion loss in the passband can be calculated as [11]

$$L = 4.34 \frac{f_0}{B} \sum_{i=1}^{2} \frac{g_i}{Q_{0i}} = 0.296 \text{ dB} \tag{27}$$

where $Q_{0i} = 580$ (experimental data) was used. Experimentally obtained transmission loss (0.15 dB of the external

microstrip line) should be added to the above calculated insertion loss to compare it with the experimental result of 0.48 dB.

The measured responses are shown in Fig. 17. The 3.332-GHz resonant frequency, 0.48-dB insertion loss, and 118-MHz bandwidth of the fabricated filter are almost the same as the design values.

IX. Conclusion

This paper presented a thorough investigation of resonant frequency, conductor Q factor, dielectric Q factor, and radiation Q factor of a $\lambda/4$ resonator. In light of the above investigation, we can conclude that a $\lambda/4$ dielectric waveguide resonator can be used as a counterpart of a $\lambda/2$ resonator, expecting similar characteristics. The OEF of the resonator can be used for resonator excitation, frequency tuning, and dual-mode coupling to fabricate a filter. The advantage of a $\lambda/4$ resonator includes more compact size and versatile use of its OEF.

Finally, we have designed and fabricated a dual-mode bandpass filter. The fabricated filter has shown an excellent coincidence with the designed values, i.e., center frequency, bandwidth, and insertion loss.

Acknowledgment

The authors would like to express their sincere gratitude to Y. Oda for carrying out the FDTD program and Prof. Y. Cho and Prof. H. Kanaya for their valuable comments and suggestions regarding this paper. The authors are also indebted to Ube Industries, Ube, Japan, for supplying dielectric materials and other technical support.

References

[1] I. Awai and T. Yamashita, "A dual mode dielectric waveguide resonator and its application to bandpass filter," *Trans. IEICE*, vol. E78-C, no. 8, pp. 1018–1024, Aug. 1995.

[2] C. Wang, B. Q. Gao, and C. P. Deng, "Accurate study of Q-factor of resonator by finite-difference time-domain method," *IEEE Trans. Microwave Theory Tech.*, vol. 43, pp. 1524–1529, July 1995.

[3] R. N. Simons, N. I. Dib, and L. P. B. Katehi, "Modeling coplanar stripline discontinuities," *IEEE Trans. Microwave Theory Tech.*, vol. 44, pp. 711–716, May 1996.

[4] M. A. W. Miah, *Fundamentals of Electromagnetics*. New York: McGraw-Hill, 1982.

[5] A. Taflove, *Computational Electrodynamics*. Norwood, MA: Artech House, 1995.

[6] D. Kajfez and P. Guillon, *Dielectric Resonators*. Norwood, MA: Artech House, 1986.

[7] I. Awai, A. C. Kundu, and T. Yamashita, "Quality factor of a $\lambda/4$ dielectric waveguide resonator and its application to a bandpass filter," in *Proc. ICEMI*, vol. 9, Shanghai, China, Oct. 1995, pp. 41–44.

[8] R. F. Harrington, *Time-Harmonic Electromagnetic Fields*. New York: McGraw-Hill, 1961.

[9] Y. Konishi, "Novel dielectric waveguide components-microwave applications of new ceramic materials," *Proc. IEEE*, vol. 79, pp. 726–740, June 1991.

[10] G. Matthaei, L. Young, and E. M. T. Jones, *Microwave Filters, Impedance—Matching Networks, and Coupling Structures*. Norwood, MA: Artech House, 1985.

[11] S. B. Cohn, "Dissipation loss in multiple-coupled-resonator filters," *Proc. IRE*, pp. 1342–1348, Aug. 1959.

Arun Chandra Kundu (S'95) received the B.S. degree in electrical engineering from Bangladesh University of Engineering and Technology, Dhaka, Bangladesh, in 1989, the M. S. degree in electrical engineering from Yamaguchi University, Ube, Japan, in 1996, and is currently working toward the Ph.D. degree.

His research interest is on microwave dielectric waveguide devices.

Ikuo Awai (M'78) received the B.S., M.S, and Ph.D. degrees from Kyoto University, Kyoto, Japan, in 1963, 1965, and 1978, respectively.

In 1968, he joined the Department of Electronics, Kyoto University, as a Research Associate, where he was engaged in microwave magnetic waves and integrated optics. From 1984 to 1990, he worked for Uniden Corporation, developing microwave communication equipments. In 1990, he joined Yamaguchi University, Ube, Japan, as a Professor, and has studied magnetostatic-wave devices, dielectric waveguide components, and superconducting devices for microwave application.

Dr. Awai is a member of the IEEE Microwave Theory and Techniques, IEEE Antennas and Propagation, and IEEE Magnetics Societies.